9084 *Biochemistry* **2009,** *48,* 9084–9093
DOI: 10.1021/bi9010495

BIOCHEMISTRY
including biophysical chemistry & molecular biology
Article

Kinetics of Association and Dissociation of HIV-1 Reverse Transcriptase Subunits†

Carl F. Venezia,‡ Brendan J. Meany,§ Valerie A. Braz,§ and Mary D. Barkley*,‡,§

§*Department of Chemistry and* ‡*Department of Physiology and Biophysics, Case Western Reserve University, 10900 Euclid Avenue, Cleveland, Ohio 44106*

Received June 20, 2009; Revised Manuscript Received August 5, 2009

ABSTRACT: The biologically active form of HIV-1 reverse transcriptase (RT) is the p66/p51 heterodimer. The process of maturation of the heterodimer from precursor proteins is poorly understood. Previous studies indicated that association of p66 and p51 is very slow. Three techniques, a pre-steady-state activity assay, intrinsic tryptophan fluorescence, and a FRET assay, were used to monitor the dimerization kinetics of RT. Kinetic experiments were conducted with purified p66 and p51 proteins in aqueous buffer. All three techniques gave essentially the same results. The dissociation kinetics of p66/p51 were first-order with rate constants (k_{diss}) of $\sim 4 \times 10^{-6}$ s^{-1} ($t_{1/2}$ = 48 h). The association kinetics of p66 and p51 were concentration-dependent with second-order rate constants (k_{ass}) of ~ 1.7 M^{-1} s^{-1} for the simple bimolecular association reaction. The implications of slow dimerization of p66/p51 for the maturation process are discussed. A reaction-controlled model invoking conformational selection is proposed to explain the slow protein−protein association kinetics.

HIV-1[1] reverse transcriptase is a critical player in the life cycle of HIV, the virus that causes AIDS. This multifunctional enzyme catalyzes three reactions: RNA- and DNA-dependent DNA polymerization and RNA hydrolysis. RT is an asymmetric heterodimer composed of two subunits, p66 and p51 (*2*). The structural asymmetry is quite astonishing considering that the two subunits are products of the same gene and exhibit identical N-terminal amino acid sequences (*3*). The p66 subunit contains both a polymerase and an RNase H domain. The polymerase domain comprises four subdomains: fingers, palm, thumb, and connection. The p51 subunit contains the same four N-terminal subdomains as p66 but lacks the C-terminal RNase H domain (*4*). The four subdomains common to the two subunits have different orientations relative to one another in the RT structure (*5*). The p66 subunit is described as having a flexible "open" conformation which contains the polymerase active site (*6*), while the p51 subunit has a compact "closed" conformation that conceals the active site residues, making it catalytically inactive (*7*). The subunit interactions are also asymmetric; the interfaces of p66 and p51 use completely different amino acid residues. Even contacts made between the connection subdomains of each subunit use entirely separate surfaces (*5*). Two models have been proposed for heterodimer formation: a concerted model in which p66 and p51 are cleaved by HIV protease from separate gag-pol precursors and a sequential model in which the RNase H domain is cleaved from one subunit of a p66/p66 homodimer intermediate (*8*). Further investigation of these subunit interactions is vital to understanding the mechanism of RT heterodimer maturation.

Previous studies of the dimerization kinetics of RT, using a combination of polymerase activity and fluorescence, proposed that subunit association is a two-step process (Scheme 1). The initial phase involves a rapid bimolecular association of p66 and p51 (10^4 M^{-1} s^{-1}) to form an inactive heterodimeric intermediate, p66*p51, followed by slow isomerization (10^{-5} s^{-1}) to the catalytically active heterodimer p66/p51 (*9*−*11*). Subunit dissociation was monophasic with a dissociation rate constant on the order of 10^{-3} s^{-1} (*11*, *12*). The studies described above achieved subunit dissociation of RT by addition of acetonitrile and subsequent subunit association by dilution of the resulting monomeric subunits into aqueous buffer. However, RT dissociation in the absence of acetonitrile was considerably slower (*13*), suggesting that acetonitrile may have an effect on the dimerization kinetics.

This paper presents the dimerization kinetics of RT in aqueous solution using separately prepared p66/p51, p66, and p51 proteins. Our prior thermodynamic study of RT subunit equilibria allows us to design kinetic experiments without resorting to organic solvent (*1*). With knowledge of homo- and heterodimer dissociation constants, reactions are set up at appropriate protein concentrations to monitor RT heterodimer dissociation or association. Three complementary techniques, including a pre-steady-state activity assay, intrinsic tryptophan fluorescence, and FRET, are used to monitor the dimerization kinetics of RT. These three techniques report protein structure in different parts of the enzyme. The implications of these findings for the maturation of the RT heterodimer are discussed.

EXPERIMENTAL PROCEDURES

Materials. A488 C_5-maleimide and QSY9 C_5-maleimide were purchased from Invitrogen (Eugene, OR). Oligodeoxynucleotides were purchased from Operon Technologies (Alameda, CA).

†This work was supported by National Institutes of Health (NIH) Grant GM071267. C.F.V. was supported by NIH Training Grant HL07653.

*To whom correspondence should be addressed. Telephone: (216) 368-0602. Fax: (216) 368-0604. E-mail: mdb4@case.edu.

[1]Abbreviations: A488, Alexa Fluor 488; ANS, 1-anilino-8-naphthalenesulfonate; DCM, dichloromethane; DTT, dithiothreitol; EDTA, ethylaminediaminetetraacetic acid; FRET, Förster resonance energy transfer; HIV-1, human immunodeficiency virus type 1; NATA, *N*-acetyltryptophanamide; NTA, nitrilotriacetic acid; PDB, Protein Data Bank; p66-A488, $p66^{S3C/C38V/C280S}$ labeled with A488; p66-QSY9, $p66^{S3C/C38V/C280S}$ labeled with QSY9; p51-A488, $p51^{S3C/C38V/C280S}$ labeled with A488; p51-QSY9, $p51^{S3C/C38V/C280S}$ labeled with QSY9; RT, reverse transcriptase; TCEP, tris(2-carboxyethyl)phosphine; Tris, tris(hydroxymethyl)aminomethane.

 Published on Web 08/28/2009

Scheme 1: Two-Step Dimerization Mechanism

$$\text{p66} + \text{p51} \underset{k_{-1}}{\overset{k_1}{\rightleftharpoons}} \text{p66*p51} \underset{k_{-2}}{\overset{k_2}{\rightleftharpoons}} \text{p66/p51}$$

dCTP (>99% purity) was from Pharmacia (Peapack, NJ). [γ-^{33}P]ATP was from PerkinElmer Life Sciences (Boston, MA). Biochemical reagents were purchased from Roche Applied Science (Indianapolis, IN). Other chemicals were purchased from Sigma Chemicals (St. Louis, MO) and Fisher Scientific (Pittsburgh, PA). RT buffer D consists of 0.05 M Tris (RNase, DNase free; pH 7.0), 25 mM NaCl, 1 mM EDTA, and 10% (v/v) glycerol (molecular biology grade, redistilled). RT buffer D used for kinetic experiments monitored by enzymatic activity and tryptophan fluorescence also contained 1 mM TCEP; the final pH was 7.0. RT reaction buffer consists of 0.05 M Tris (pH 7.8), 0.01 M $MgCl_2$, 0.08 M KCl, and 5 mM DTT. PBS buffer consists of 137 mM NaCl, 11.9 mM phosphates (pH 7.4), and 2.7 mM KCl. TBE buffer consists of 0.089 M Tris, 0.089 M boric acid (pH 8.0), and 2 mM EDTA. Loading buffer consists of 90% formamide, 10% 10× TBE, 0.025% bromophenol blue, and 0.025% xylene cyanol. The acrylamide solution in TBE contains a 20% acrylamide/bisacrylamide mixture (19:1) and 7.8 M urea.

Synthesis of N-Acetylcysteine-A488. *N*-Acetylcysteine (0.5 mg, 81.1 mmol) was placed in a 1.5 mL microcentrifuge tube and dissolved in 0.5 mL of methanol. A488 C_5-maleimide (1.5 equiv, 123.0 mmol) was added, and the reaction solution was mixed for 1.5 h at room temperature. Upon completion of the reaction, the volume was reduced under vacuum and the product was purified via silica gel flash chromatography. The crude reaction mixture was loaded onto an 8 cm × 0.5 cm column equilibrated with DCM. The column was washed with 4 column volumes of a 4:1 DCM/methanol mixture to elute any residual starting materials and then with a 1:2 DCM/methanol mixture to obtain the clean product.

Protein Preparation. RT proteins were purified as described previously (*1*, *14*). The protein concentration is determined from the absorbance at 280 nm (*1*, *15*). All RT protein concentrations are expressed as monomer.

RT proteins with a single cysteine at position 3 were prepared from two plasmids containing the S3C/C38V/C280S triple mutation. The S3C mutation was introduced into a plasmid containing the C38V/C280S double mutation using the QuikChange II site-directed mutagenesis kit (Stratagene, La Jolla, CA): p6H RT$^{C38V/C280S}$ for p66 and p6H RT51$^{C38V/C280S}$ for p51 (*1*). Mutagenic oligonucleotide primer sequences for the S3C mutation were as follows: forward, 5′-GTACAGTCTCAATAGGGCAAATGGGAAGCTGGGATC-3′; reverse, 5′-GATCCCAGCTTCCCATTTGCCCTATTGAGACTGTAC-3′. All mutations were confirmed by DNA sequencing at Cleveland Genomics (Cleveland, OH).

Mutated proteins p66$^{S3C/C38V/C280S}$ and p51$^{S3C/C38V/C280S}$ were labeled with either A488 or QSY9 maleimide using the following procedure. The protein was treated with a 4-fold molar excess of DTT overnight at 5 °C followed by dialysis into PBS for 3 h. A fresh stock solution of maleimide probe was prepared in dimethylformamide. The protein was reacted for 1 h at room temperature three times with a 10-fold excess of A488 maleimide or a 5-fold excess of QSY9 maleimide. Labeled protein was then affixed to 0.5 mL of Ni-NTA Superflow resin (Qiagen, Valencia, CA) in a 3 mL disposable column (Pierce, Rockford, IL) and washed with PBS containing 25 mM imidazole until the absorbance at 495 nm reached <0.005. The column was capped on the bottom, and 0.5 mL of PBS containing 0.3 M imidazole was added; after gentle agitation, the column was allowed to sit for 20 min. Labeled protein was eluted with PBS containing 0.3 M imidazole, concentrated against sucrose, and dialyzed into RT buffer D. The labeling stoichiometry was estimated from absorption spectra using extinction coefficients $\varepsilon(495)$ of 7.1×10^4 M^{-1} cm^{-1} for A488 and $\varepsilon(562)$ of 8.8×10^4 M^{-1} cm^{-1} for QSY9 (*16*, *17*). Molar ratios of protein to probe were 1.0−1.08. Labeling specificity was confirmed by tandem mass spectrometry using a LCQ Deca XP Max ion trap mass spectrometer (Thermo Finnigan, San Jose, CA).

Pre-Steady-State Activity Assay. The RT dimer concentration was determined by active site titration at saturating DNA substrate concentrations. The 25/36-mer random sequence DNA described previously was used as a substrate (*18*). The oligonucleotides were purified; the duplex was annealed, purified, and 5′-end labeled with [γ-^{33}P]ATP (*19*). The DNA concentration was determined from the absorbance at 260 nm (*15*). Ten microliters of the RT solution was mixed with 90 μL of RT reaction buffer containing 1 μM DNA substrate and 0.1 mM dCTP at 37 °C. Aliquots (5 μL) were removed and mixed with 5 μL of 0.1 M EDTA to quench the reaction. Time points were taken at 20 s intervals for the first 4 min and at 1 min intervals for an additional 4 min. The remaining reaction mixture was left overnight at 37 °C to go to completion, and a final time point was taken to determine the 3′-OH concentration. Ten microliters of loading buffer was added to the quenched reaction mixtures, and products were separated on a 20% denaturing polyacrylamide gel. The gel was exposed on a phosphorimaging screen (Bio-Rad Laboratories, Hercules, CA); the resulting image was quantified using a Storm Phosphorimager (Molecular Dynamics, Piscataway, NJ) and OptiQuant software (Packard Instrument Co., Meriden, CT), and the reaction was quantified as described previously (*18*). The time course of dCMP addition y was fit by linear regression to

$$y = B + k_{ss}t \quad (1)$$

where B is the burst amplitude at time zero and k_{ss} is the steady-state rate. The burst amplitude is the active enzyme concentration in dimer units, because one heterodimer binds per labeled DNA; [p66/p51] = 2B, where [p66/p51] is in monomer units.

Dissociation and association kinetics of p66/p51 were measured in RT buffer D at 5 °C. Dissociation reactions were started by 200-fold dilution of a 10 μM solution of p66/p51 to 50 nM, so that reassociation can be ignored in the data analysis. After dilution, 10 μL aliquots were assayed at 0.17, 0.5, 1, 2, 3, and 6 h; every 6 h until 36 h; every 12 h until 96 h; every 12−96 h; and then every 24 h to 10 days. The burst amplitudes $B(t)$ at various times t after dilution of p66/p51 were fit to

$$B(t) = C_1 \exp(-k_{diss}t) + C_2 \quad (2)$$

where k_{diss} is the dissociation rate constant and the C_i terms are constants. Association reactions were started by mixing equal volumes of 1 μM p66 with either 1 or 5 μM p51; 10 μL aliquots of the reaction mixture were assayed at ≥1 h intervals for up to 10 days. At early times, the bimolecular p66 + p51 → p66/p51 association can be assumed to be an irreversible reaction, and

an association rate constant k_{ass} can be calculated from the slope of the integrated rate equations. For equal initial concentrations, $[p66]_0$ and $[p51]_0$

$$\frac{[p66/p51]}{[p51]_0([p51]_0 - [p66/p51])} = k_{ass}t \quad (3)$$

and for unequal initial concentrations

$$\frac{1}{[p51]_0 - [p66]_0} \ln \frac{[p66]_0([p51]_0 - [p66/p51])}{[p51]_0([p66]_0 - [p66/p51])} = k_{ass}t \quad (4)$$

An observed rate constant k_{obs} was obtained by fitting $B(t)$ at time t after mixing p66 and p51 to

$$B(t) = C[1 - \exp(-k_{obs}t)] \quad (5)$$

where C is a constant. The association kinetics are exponential only under pseudo-first-order conditions.

Steady-State Fluorescence. Absorbance was measured on a Cary 3E UV−vis spectrophotometer at 5 °C. Fluorescence was measured on a PC1 Photon Counting spectrofluorometer (ISS, Champaign, IL) in ratio mode under magic angle conditions using 4 nm excitation and 16 nm emission band-pass. The temperature was maintained at 5 °C by a TC 425 Peltier unit (Quantum Northwest, Liberty Lake, WA), and the sample compartment was flushed with nitrogen to prevent condensation. Samples were placed in 45 μL quartz cells with a path length of 3 mm (Starna Cells, Inc., Atascadero, CA). Absorbance at the long wavelength maximum was < 0.3 to avoid inner filter effects. Fluorescence quantum yields (Φ) were measured relative to fluorescein in 0.1 M NaOH at an excitation wavelength of 450 nm and 5 °C. A value of 0.95 at 22 °C was used for the quantum yield of fluorescein (*20*).

Dissociation and association kinetics of p66/p51 in RT buffer D were monitored by fluorescence using Vinci 1.6.SP7 (ISS). Fast kinetic intensity data were collected from samples and a reference fluorophore every 5 s (signal averaged over 1 s) for the first 2 h. This was followed by one 16 h period of slow data acquisition every 5 min (signal averaged over 10 s) and subsequent 24 h periods for 6−10 days. Reactions of samples containing two labeled subunits were conducted simultaneously with a control reaction containing one A488-labeled subunit and one unlabeled subunit, and the background fluorescence from the control reaction was subtracted. Fluorescence intensity F ($= I_s/I_r$) was calculated from the ratio of sample intensity I_s to reference intensity I_r to correct for instrumental drift.

Intrinsic tryptophan fluorescence was measured at with excitation and emission wavelengths of 295 and 340 nm, respectively, using NATA in water as a reference. The A488 fluorescence was measured at excitation and emission wavelengths of 450 and 540 nm, respectively, using fluorescein in 0.1 M NaOH as a reference. Dissociation reactions were started by 200-fold dilution of a 10 μM solution of unlabeled or labeled p66/p51. Association reactions were started by mixing equal volumes of 1 μM solutions of unlabeled or labeled p66 with 1−5 μM solutions of unlabeled or labeled p51. Samples were mixed in the cell and placed in the fluorometer within 5 s. The fractional fluorescence increase or decrease due to dissociation or association of RT was fit to an exponential function.

$$[F(t) - F_0]/(F_\infty - F_0) = C[1 - exp(-k_{diss}t)] \quad (6a)$$

$$[F(t) - F_\infty]/(F_0 - F_\infty) = C_1\, exp(-k_{obs}t) + C_2 \quad (6b)$$

where F_0 is the intensity at time zero, $F(t)$ is the intensity at time t, and F_∞ is the intensity of the last time point. Here too, the association kinetics are exponential only under pseudo-first-order conditions.

Time-Resolved Fluorescence. Fluorescence lifetimes were measured by time-correlated single-photon counting as described previously (*21*). Decay data were collected at excitation and emission wavelengths of 450 and 540 nm, respectively, in 1024 channels of 18 and 24 ps/channel. Intensity decays $I(t)$ with amplitudes α_i and lifetimes τ_i were fit to sums of exponentials.

$$I(t) = \sum_i \alpha_i \exp(-t/\tau_i) \quad (7)$$

Decay curves on different time scales were deconvolved by global analyses with the lifetimes linked. Amplitude-weighted lifetimes $\bar{\tau}$ are calculated from

$$\bar{\tau} = \sum_i \alpha_i\tau_i / \sum_i \alpha_i \quad (8)$$

Fractional intensities f_i of individual decay components were calculated from lifetime data and the relative steady-state intensity $F(540)$ at 540 nm.

$$f_i = \alpha_i\tau_i F(540) / \sum_i \alpha_i\tau_i \quad (9)$$

RESULTS

RT subunits undergo three coupled dimerization reactions in solution:

$$p66 + p51 = p66/p51 \quad (10a)$$

$$p66 + p66 = p66/p66 \quad (10b)$$

$$p51 + p51 = p51/p51 \quad (10c)$$

with a K_d(p66/p51) of 310 nM, a K_d(p66/p66) of 4.2 μM, and a K_d(p51/p51) of 230 μM (*1*).[2] The relative concentrations of the three dimeric species must be taken into consideration when designing kinetic experiments. The RT concentrations can be calculated from eqs 10a−10c using Mathematica as described previously (*1*).

Kinetics Monitored by Enzymatic Activity. Dimerization is absolutely required for both the DNA polymerase and RNase H activities of RT (*10*, *22*). Monomeric forms of RT are not catalytically active and do not bind primer/template substrate (*15*). In the pre-steady-state assay, the time course of a single-nucleotide addition experiment has a rapid initial burst followed by a slow linear steady-state phase (Figure 1, top panel inset). The slope of the steady-state phase is steady-state rate k_{ss}; the intercept is burst amplitude B, which gives the amount of active enzyme at saturating concentrations of DNA substrate. For all experiments, the burst phase occurred within the first 2 min of each 8 min reaction. Thus, a pre-steady-state assay at each time point in the dimerization reaction measures dimer concentration directly, unlike the conventional steady-state DNA polymerase assay.

Dissociation kinetics for RT were determined under irreversible conditions using a concentration jump to a value lower than

[2]These values were determined in RT buffer D containing 1 mM TCEP, which was added after pH had been adjusted (*1*). The addition of TCEP lowered the pH to 6.5.

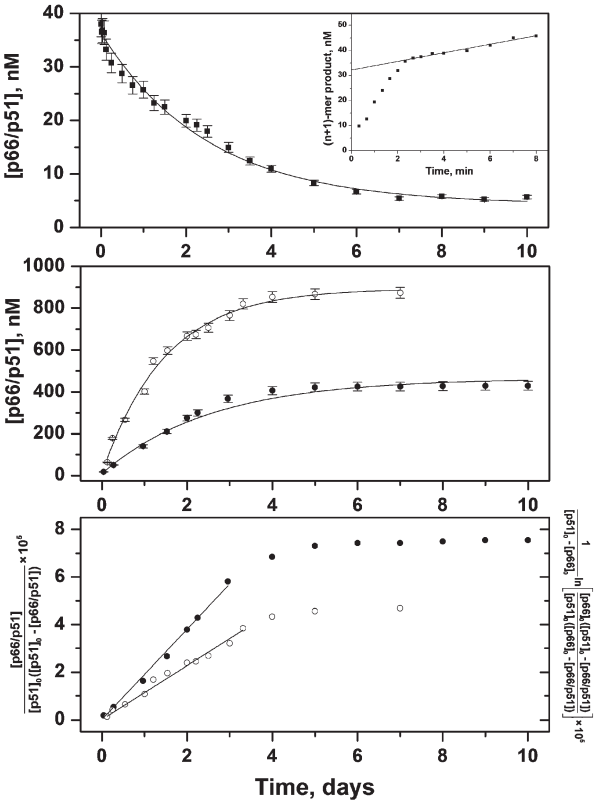

FIGURE 1: Kinetics of RT subunit dissociation and association monitored by a pre-steady-state activity assay. Error bars are standard deviations of at least three experiments. The top panel shows dissociation of 50 nM p66/p51 at various times (■) fit to eq 2 (—). The inset shows a time course of single-nucleotide addition to DNA substrate. The slope of the line is steady-state rate k_{ss}; the intercept is burst amplitude B ([p66/p51]/2). The middle panel shows association of 0.5 μM p66 with 0.5 μM p51 (●) and 0.5 μM p66 with 2.5 μM p51 (○) fit to eq 5 (solid lines). The bottom panel shows association of 0.5 μM p66 with 0.5 μM p51 (●) fit to eq 3 and 0.5 μM p66 with 2.5 μM p51 (○) fit to eq 4.

K_d to induce dissociation. The lower limit for detection in the pre-steady-state assay was established to be less than 5 nM of an equilibrated solution of RT heterodimer. In an equilibrated solution of p66/p51 where $[\text{monomer}]_{tot}$ = 10 μM, 74% of the total monomer is heterodimer: [p66/p51] = 7.4 μM, [p66/p66] = 0.38 μM, [p51/p51] = 0.022 μM, [p66] = 0.9 μM, and [p51] = 1.3 μM. This compares to an equilibrated solution where $[\text{monomer}]_{tot}$ = 50 nM, in which only 6.8% of total monomer is heterodimer: [p66/p51] = 3.4 nM, [p66/p66] = 0.24 nM, [p51/p51] = 0.0048 nM, [p66] = 23 nM, and [p51] = 23 nM. Each dissociation experiment was performed three times, and burst amplitudes for the same time point were averaged and plotted versus time (Figure 1, top panel). Active p66/p51 concentrations approach but never reach zero because 50 nM RT is 6.8% heterodimer at equilibrium. The dissociation data were analyzed with eq 2 assuming a first-order reaction

$$-d[p66/p51]/dt = k_{diss}[p66/p51] \quad (11)$$

with a dissociation rate constant k_{diss} of (4.4 ± 0.2) × 10^{-6} s^{-1} (Table 1).

To study association kinetics, the initial solutions of p66 and p51 should be sufficiently dilute to ensure predominantly monomers prior to mixing but sufficiently concentrated to form a heterodimer after mixing. We compromised with a 1 μM solution of p66, in which [p66/p66] = 0.13 μM, and a 5 μM solution of p51, in which [p51/p51] = 37 nM. After equal volumes of these solutions had been mixed, $[\text{monomer}]_{tot}$ = 3 μM; at equilibrium, 90% of the p66 will be heterodimer: [p66/p51] = 900 nM, [p66/p66] = 2 nM, [p51/p51] = 51 nM, [p66] = 47 nM, and [p51] = 2 μM. Burst phases typically occurred within the first 3 min of each reaction. Burst amplitudes for the same time points from three association reactions were averaged and plotted versus time (Figure 1, middle panel, empty symbols). In the top curve, active p66/p51 concentrations never go above 900 nM, because only 90% of p66 is heterodimer at equilibrium. Analogous experiments with p66 in excess of p51 were not performed because an equilibrated solution of 5 μM p66 is 53% homodimer. However, experiments were performed using 1 μM solutions of p66 and p51 to determine the molecularity of the association reaction and facilitate comparison with tryptophan fluorescence experiments (Figure 1, middle panel, filled symbols). At these monomer concentrations, [p66/p51] = 440 nM at equilibrium. For a simple reversible association reaction (Scheme 2)

$$d[p66/p51]/dt = k_{ass}[p66][p51] - k_{diss}[p66/p51] \quad (12)$$

The data at early times in the association reactions were fit to integrated rate equations for a second-order reaction (eqs 3 and 4; Figure 1, bottom panel). k_{ass} = 2.2 ± 0.2 M^{-1} s^{-1} for equal initial concentrations, and k_{ass} = 1.3 ± 0.2 M^{-1} s^{-1} for unequal initial concentrations. The entire time courses were fit to eq 5 to produce observed rate constants (k_{obs}) of (5.8 ± 0.2) × 10^{-6} and (7.8 ± 0.3) × 10^{-6} s^{-1}. For a simple association equilibrium

$$k_{obs} = k_{diss} + k_{ass}[p51] \quad (13)$$

The concentration dependence of k_{obs} indicates that the rate-limiting step for association of RT subunits is bimolecular. The association rate constant (k_{ass}) was calculated from the k_{obs} of (7.8 ± 0.3) × 10^{-6} s^{-1} determined under pseudo-first-order conditions using eq 13 where [p51] = $[p51]_0$ = 5 μM, giving a k_{ass} of 1.4 ± 0.2 M^{-1} s^{-1} in agreement with the value calculated using eq 4 (Table 1).

Kinetics Monitored by Tryptophan Fluorescence. The RT heterodimer contains 37 Trp residues distributed throughout the structure, any of which may report a conformational change due to dimerization (Figure 2). A cluster of six Trps in the connection subdomain has been shown to play a major role in dimerization (*23*, *24*). As reported previously, the dissociation of the RT heterodimer with 20% acetonitrile is accompanied by a 25% increase in the tryptophan fluorescence intensity and a shift in the emission spectrum from 338 to 345 nm (*11*). In the absence of acetonitrile, the fluorescence intensity changes due to dimerization are ~25% with no shift in the emission maximum of 337 nm. We exploited this change in tryptophan fluorescence intensity to determine the dissociation and association kinetics of RT under conditions identical to those of the pre-steady-state assay. The fractional increase or decrease in fluorescence intensity is plotted versus time in Figure 3. The dissociation data were fit to eq 6a to produce a k_{diss} of (3.9 ± 0.3) × 10^{-6} s^{-1} (Figure 3, top panel), within error of the value measured in the pre-steady-state assay (Table 1). However, inspection of Figure 3 (top panel) shows that a single exponential does not adequately fit the data for the first 8 h. A better fit is obtained by including a second exponential term in eq 6a, which gives a $k_{diss}(1)$ of (3.6 ± 0.4) × 10^{-6} s^{-1} and a $k_{diss}(2)$ of (7.6 ± 0.5) × 10^{-5} s^{-1} with relative amplitudes of 0.72 ± 0.1 and 0.28 ± 0.1, respectively. The slower rate constant, $k_{diss}(1)$, which is the major component, is approximately the same

Table 1: Dissociation and Association Rate Constants of Wild-Type RT[a]

method	protein solutions[b]	k_{diss} ($\times 10^{-6}$ s^{-1})	k_{obs} ($\times 10^{-6}$ s^{-1})	k_{ass} (M^{-1} s^{-1})
		Dissociation Reaction		
pre-steady-state assay	50 nM p66/p51	4.4 ± 0.2		
Trp fluorescence[c]	50 nM p66/p51	3.9 ± 0.3		
		Association Reaction		
pre-steady-state assay	0.5 μM p66, 0.5 μM p51		5.8 ± 0.2	2.2 ± 0.2[d]
	0.5 μM p66, 2.5 μM p51		7.8 ± 0.3	1.3 ± 0.2[e]
				1.4 ± 0.2[f]
Trp fluorescence[c]	0.5 μM p66, 0.5 μM p51		5.4 ± 0.4	

[a]RT buffer D with 1 mM TCEP, at 5 °C. Errors are standard deviations of three to nine experiments. [b]Final concentrations. [c]λ_{ex} = 295 nm, and λ_{em} = 340 nm. [d]Calculated from eq 3. [e]Calculated from eq 4. [f]Calculated from eq 13.

Scheme 2: Bimolecular Dimerization Mechanism

$$\text{p66} + \text{p51} \underset{k_{diss}}{\overset{k_{ass}}{\rightleftharpoons}} \text{p66/p51}$$

as the value obtained from the single-exponential fit; the minor component, $k_{diss}(2)$, is 20-fold higher.

For the association reaction, the fluorescence intensity was measured at 5 s intervals in an attempt to resolve a fast bimolecular step. However, as seen in Figure 3 (inset), the fluorescence did not change detectably for the first 2 h after mixing. The association data measured at 5 min intervals were fit to eq 6b to produce a k_{obs} of $(5.4 \pm 0.4) \times 10^{-6}$ s^{-1}, in good agreement with the value obtained from enzymatic activity (Table 1). However, because p66 has 19 Trp residues and p51 has 18 Trp residues, it proved to be impossible to use excess p51 to achieve pseudo-first-order conditions. In an experiment using 1 μM p66 and 3 μM p51, the excess p51 contributed sufficient background fluorescence to obscure the decrease in fluorescence due to dimerization. Figure 3 (bottom panel) shows that a single exponential does not adequately fit the data for the first 12 h. A better fit is obtained here as well by including a second exponential term in eq 6b, which gives a $k_{obs}(1)$ of $(2.3 \pm 0.1) \times 10^{-6}$ s^{-1} and a $k_{obs}(2)$ of $(2.1 \pm 0.2) \times 10^{-5}$ s^{-1} with relative amplitudes of 0.70 ± 0.1 and 0.30 ± 0.1, respectively. The slower rate constant, $k_{obs}(1)$, which is the major component, is a factor of 2.3 lower than the value obtained from the single-exponential fit; the minor component, $k_{obs}(2)$, is 4-fold higher.

Kinetics Monitored by FRET. The 10 N-terminal residues of both subunits are loops in the crystal structure of the heterodimer (Figure 2). We attached fluorescence probes to a single cysteine at position 3 of the RT sequence. These labeled proteins were used in a FRET assay with A488/QSY9 as the donor/acceptor pair. The Förster distances (R_0) are 60 Å for p66-A488/p51-QSY9 and 59 Å for p66-QSY9/p51A-488, assuming a random orientation of the transition dipoles (*25*). This compares to a distance of ~40 Å between the S3 residues of p66 and p51 in the crystal structure (*26*). The A488 donor has high photostability and quantum yield; the QSY9 acceptor is nonfluorescent, which eliminates background fluorescence due to direct excitation of the acceptor. Therefore, the fluorescence intensity of A488 should be highly quenched in the heterodimer relative to the monomers. The top panel of Figure 4 displays the dissociation kinetics of the heterodimer after dilution of p66-A488/p51-QSY9 and of p66-QSY9/p51-A488. A control reaction of heterodimer with donor alone was run in parallel to correct for any change in donor fluorescence due to a protein conformational change. The values of the dissociation rate constant obtained by fitting these data to eq 6a were independent within error of the position of the labels: $k_{diss} = (2.5 \pm 0.5) \times 10^{-6}$ s^{-1} for p66-A488/p51-QSY9 and $k_{diss} = (1.9 \pm 0.4) \times 10^{-6}$ s^{-1} for p66-QSY9/p51-A488 (Table 2). The dissociation rate constants of the labeled RT are a factor of ~2 lower than for wild-type RT.

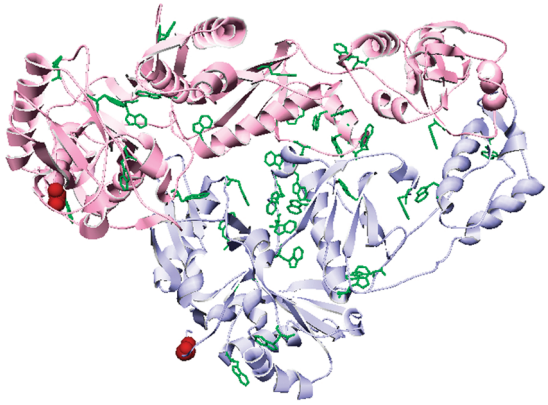

FIGURE 2: Ribbon diagram of unliganded HIV-1 p66/p51 RT (PDB entry 1DLO; pink for p66, blue for p51). Tryptophan side chains are colored green; labeling sites are colored red, using the van der Waals radius of S3.

The bottom panel of Figure 4 shows the association data from experiments mixing p66-A488 with p51-QSY9 and p66-QSY9 with p51-A488. The fluorescence intensity did not change for the first 2 h after 1 μM solutions of the two subunits had been mixed (inset), and the observed rate constant (k_{obs}) obtained from the fit to eq 6b was independent of labeling position (Table 2). Additional experiments were performed under pseudo-first-order conditions, using 1 μM p66-A488 and 3−5 μM p51-QSY9. As expected for a bimolecular reaction, the value of the observed rate constant (k_{obs}) is concentration-dependent (Table 2). The association rate constant (k_{ass}) of 1.7 M^{-1} s^{-1} calculated from eq 13 for labeled RT agrees well with the value for wild-type RT (Table 1).

DISCUSSION

RT heterodimer maturation is a complex process that, despite its importance, is not understood. Central to this process are the interactions of its subunits. The concentration of RT in the virion, estimated from the number of RT molecules and the size

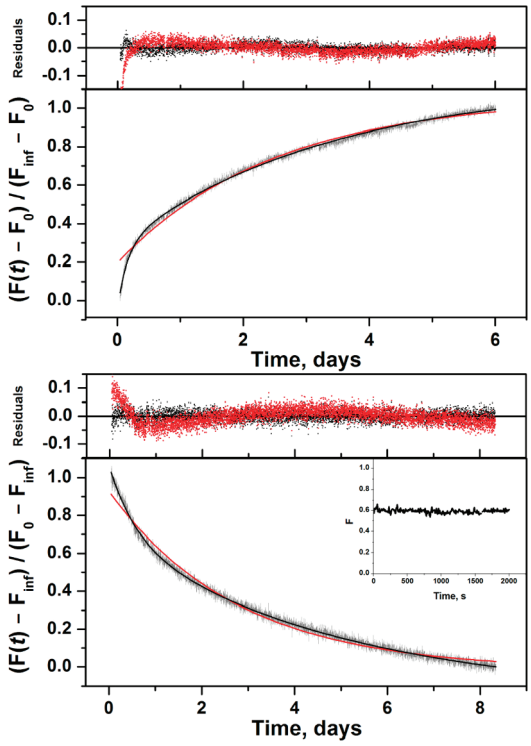

FIGURE 3: Kinetics of RT subunit dissociation and association monitored by intrinsic tryptophan fluorescence. The top panel shows dissociation of 50 nM p66/p51 fit to eq 6a (red line) and eq 6a with a second exponential term (black line). Residuals for both fits are shown above. The bottom panel shows association of 0.5 μM p66 and 0.5 μM p51 fit to eq 6b (red line) and eq 6b with a second exponential term (black line). Residuals for both fits are shown above. The inset shows the initial 2000 s.

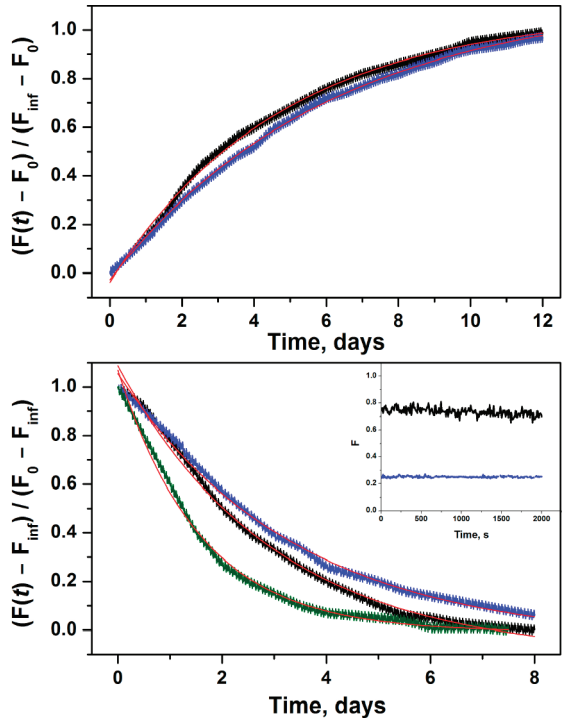

FIGURE 4: Kinetics of RT subunit dissociation and association monitored by FRET. The top panel shows dissociation of 50 nM p66-A488/p51-QSY9 (black) and 50 nM p66-QSY9/p51-A488 (blue) fit to eq 6a (red lines). The bottom panel shows association of 0.5 μM p66-A488 with 0.5 μM p51-QSY9 (black), 0.5 μM p66-QSY9 with 0.5 μM p51-A488 (blue), and 0.5 μM p66-A488 with 2.5 μM p51-QSY9 (olive) fit to eq 6b (red lines). The inset shows the initial 2000 s of 0.5 μM p66-A488 with 0.5 μM p51-QSY9 (black) and 0.5 μM p66-QSY9 with 0.5 μM p51-A488 (blue).

of the viral particle, is roughly 250 μM. At these concentrations, the dimerization reaction would be ~10^5-fold faster and occur on a time scale of minutes rather than days. A complete replication cycle of HIV takes ~48 h (*27*). RT is translated as part of the p160 gag-pol polyprotein and subsequently cleaved by the pol-encoded protease. The processing of a 90 kDa pol polyprotein to yield p66/p51 has been examined using an inducible bacterial expression vector (*8*). The full-length polyprotein was the first product formed, followed by p66; p51 appeared only after a significant amount of p66 had accumulated. Both the concerted and sequential models proposed for heterodimer formation posit a subunit dimerization step. In the concerted model, p66 and p51 associate to form the mature heterodimer. In the sequential model, p66 self-associates to form a homodimer, followed by removal of the RNase H domain from one subunit by HIV protease. These results support the sequential model. The previously reported association rate constant (k_{ass}) of 1.4×10^{-2} M^{-1} s^{-1} for formation of the p66/p66 homodimer is 2 orders of magnitude lower than the value of ~1.7 M^{-1} s^{-1} obtained here for formation of the p66/p51 heterodimer (*10*). A faster association rate constant for formation of the p66/p51 heterodimer compared to the p66/p66 homodimer suggests that RT formation may proceed via the concerted model. However, the homodimer association kinetics were measured using organic solvent (*10*). Whatever the model, these results suggest that RT heterodimer maturation appears to be a slow process. A chaperone protein in the cell may facilitate RT dimerization, but so far, no such protein has been identified. The nucleocapsid protein cleaved from the gag-pol polyprotein was a plausible candidate, though in preliminary experiments it had no effect on dimerization.

In this work, we used three techniques to monitor dimerization: enzymatic activity, tryptophan fluorescence, and FRET. These techniques report different aspects of RT structure: the presence of a primer/template binding cleft and polymerase active site; the local environment of Trp residues, presumably the tryptophan cluster in the connection subdomains; and the proximity of the N-termini of the two subunits. Our results support a simple reversible bimolecular association reaction (Scheme 2). We obtained similar values from each method for both the association and dissociation rate constants. Heterodimer dissociation is a first-order reaction with k_{diss} values of 4×10^{-6} s^{-1} for the wild-type heterodimer and 2×10^{-6} s^{-1} for the labeled heterodimer. Association of the two monomers is a second-order reaction that is dependent on monomer concentrations with a k_{ass} of $\cong$1.7 M^{-1} s^{-1}. There is no evidence of a fast bimolecular association followed by slow isomerization to active RT. If this were the case, we would have been able to observe a biphasic reaction in both the tryptophan fluorescence and FRET experiments. According to the law of mass action, the equilibrium dissociation constant K_d(p66/p51) = k_{diss}/k_{ass}. The K_d values calculated from the ratio of the rate constants are 4−10-fold larger than the value determined by sedimentation equilibrium (*1*). Possible contributions to this difference are (1) the fact that buffer pH was 7.0 in kinetic experiments compared to 6.5 in ultracentrifugation experiments[2] and (2) the fact that p66 solutions prior to mixing contained ~13% p66/p66 homodimer, which is accounted for in the K_d(p66/p51) but not in the rate constants. Protein degradation does not occur during these slow reactions, as RT is stable for at least a month in RT buffer D at 5 °C (*1*).

Table 2: Dissociation and Association Rate Constants of Labeled RT[a]

protein solution[b]	k_{diss} ($\times 10^{-6}$ s^{-1})	k_{obs} ($\times 10^{-6}$ s^{-1})	k_{ass}[c] (M^{-1} s^{-1})
	Dissociation Reaction		
50 nM p66-A488/p51-QSY9	2.5 ± 0.5		
50 nM p66-QSY9/p51-A488	1.9 ± 0.4		
	Association Reaction		
0.5 μM p66-A488, 0.5 μM p51-QSY9		4.1 ± 0.4	
0.5 μM p66-QSY9, 0.5 μM p51-A488		3.4 ± 0.4	
0.5 μM p66-A488, 1.5 μM p51-QSY9		4.8 ± 0.3	1.6 ± 0.2
0.5 μM p66-A488, 2.0 μM p51-QSY9		5.7 ± 0.4	1.6 ± 0.2
0.5 μM p66-A488, 2.5 μM p51-QSY9		7.1 ± 0.3	1.8 ± 0.4

[a]RT buffer D, at 5 °C. Errors are standard deviations of three experiments. λ_{ex} = 450 nm, and λ_{em} = 520 nm. [b]Final concentrations. [c]Calculated from eq 13.

Protein−protein association kinetics with rate constants ranging from $< 10^3$ to $> 10^9$ M^{-1} s^{-1} have been examined experimentally and theoretically (*28*). A kinetic mechanism similar to Scheme 1, which proceeds through a transient complex or kinetic intermediate, is often used to describe these systems. Diffusion-controlled rate constants, which involve local conformational changes between unbound proteins and the native complex, fall on the upper end of the time scale mentioned above, while reaction-controlled rate constants, which involve sizable domain movement-type changes, fall on the lower end. Studies of slow protein−protein interactions on the time scale of RT subunit dimerization are not unprecedented. Homodimerization of BirA, a biotin regulatory protein in *Escherichia coli*, is governed by very slow forward (k_{on} = 20 M^{-1} s^{-1}) and reverse (k_{off} = 3 × 10^{-4} s^{-1}) rate constants (*29*).

The extremely slow association of RT subunits is a quite intriguing result. RT faces the dilemma of forming asymmetric dimers from two subunits with identical amino acid sequences. HIV-1 RT is an asymmetric heterodimer in the 127 crystal structures currently available (*30*). Although there are no crystal structures of p66/p66 and p51/p51 homodimers, both of which have polymerase activity (*10*), the homodimers would also have to be asymmetric to create the primer/template binding cleft and polymerase active site. There are also no crystal structures of p66 and p51 monomers. However, hydrogen exchange mass spectrometry shows that the p51 monomer and the polymerase domain of the p66 monomer have similar solution structures (unpublished data), which are comparable to the solution structure of the p51 subunit in p66/p51 (*31*). To adopt the asymmetric structure of the heterodimer, the conformations of the p66 monomer and, to a lesser extent, the p51 monomer must change. Three models for the slow association reaction are (1) a weakly bound dimer intermediate, (2) unfavorable orientation effects, and (3) conformational selection. Model 1 postulates a two-step mechanism involving a transient complex (Scheme 1). If $k_{-1} \gg k_2$, the association reaction will exhibit second-order kinetics with a rate constant $k_{ass} \propto K_a k_2$, where K_a ($= k_1/k_{-1}$) is the equilibrium constant for formation of the complex. The slow association rate constant k_{ass} implies that K_a is very small (mM^{-1}). At the micromolar concentrations used in the kinetic experiments, the intermediate never comprises a detectable fraction of RT and occurs at such low concentrations that accumulation of the active heterodimer proceeds very slowly. Model 1 is analogous to the previously proposed mechanism based on Scheme 1, except that the isomerization k_2 from inactive to active heterodimer has to be faster than the isomerization k_{-2} from active to inactive heterodimer to observe active p66/p51. Model 2 invokes direct binding of p66 and p51 with unfavorable orientation effects (Scheme 2). The slow bimolecular step implies that productive collisions of p66 and p51 are extremely rare. Model 3 proposes conformational selection from a population of dynamic monomer structures (*32*). Only two monomers in the right conformations can combine to form the asymmetric dimer. The individual subunits undergo separate conformational changes prior to the bimolecular reaction to form the active heterodimer (Scheme 3). The unimolecular rate constants k_c and k_{-c} in this scheme would be undetectable by enzymatic activity or FRET, because these techniques monitor only dimerization. The conformational equilibrium constant K_c ($= k_c/k_{-c}$) is unfavorable, and the overall rate constant k_{ass} ($\propto K_c k_1$) is thereby slow. Because our data provide scant evidence of the complexity of either the association or dissociation kinetics, we cannot distinguish between the three models on the basis of the results in this paper. However, we prefer model 3 because of the flexibility of RT together with the different structures of the subunits in the asymmetric heterodimer (*31*). Future studies of the effects of temperature, pH, osmolytes, and mutational analysis on the dimerization kinetics will test these models.

Scheme 3: Reaction-Controlled Dimerization Mechanism

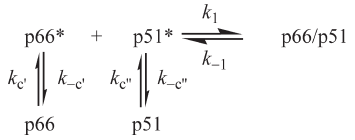

The biphasic association and dissociation kinetics resolved by tryptophan fluorescence introduce a wrinkle into these models, although the rate constants of the second minor component are still very slow. Attempts to fit the enzymatic activity and FRET data to two exponential functions failed to resolve two components with different rate constants. The deviation of the tryptophan fluorescence data from a single-exponential function is most apparent in the first 8 h of the dissociation reaction and the first 12 h of the association reaction (Figure 3). In the case of the enzymatic activity data, there are sufficient points at early times in the dissociation experiment, but not in the association experiment, to have resolved the biphasic kinetics. The data acquisition protocols for the tryptophan fluorescence and FRET experiments were identical, yet no evidence of biphasic kinetics is apparent in the FRET data. If there are two forms of heterodimer

that undergo simultaneous association and dissociation reactions, then the biphasic kinetics should be manifest by all three techniques. The minor component may represent either the conformational equilibria of the monomers in Scheme 3 or inactive heterodimer p66·p51 in Scheme 1, which associates and dissociates slowly. An inactive intermediate would not be seen by enzymatic activity; it would be seen by FRET unless the close positioning of the N-termini is one of the last conformational changes to occur.

Previously, RT dimerization kinetics were monitored by fluorescence and polymerase activity, and the results were interpreted according to the two-step mechanism in Scheme 1 (*9*−*12*). Rapid association and dissociation kinetics yielding a second-order rate constant for the first step in the association reaction ($k_1 = 2.8 \times 10^4\ M^{-1}\ s^{-1}$) and a first-order rate constant for the overall dissociation reaction [$k_d = k_{-1}k_{-2}/(k_{-1} + k_2) = 4.5 \times 10^{-3}\ s^{-1}$] were determined by tryptophan fluorescence. Slow association kinetics yielding a first-order rate constant for the second step in the association reaction ($k_2 = 3-6 \times 10^{-5}\ s^{-1}$) were observed by polymerase activity. Biphasic association kinetics monitored by ANS fluorescence were decomposed into fast and slow phases with a second-order rate constant k_1 of $3.9 \times 10^4\ M^{-1}\ s^{-1}$ and a first-order rate constant k_2 of $2.8 \times 10^{-5}\ s^{-1}$. The dimerization mechanism proposed in Scheme 1 with the rate constants mentioned above is implausible. If $k_{-1} > k_2$, then $k_d \sim k_{-2}$, and k_2 has to be larger than k_{-2} for observation of the active heterodimer. However, the overall dissociation rate constant $k_d \sim k_{-2}$ is 2 orders of magnitude faster than the rate-limiting step k_2 in the association reaction. A possible reason for the fast kinetics is the use of organic solvent to produce p66 and p51 monomers. All previous experiments achieved dissociation of p66/p51 by addition of 20% acetonitrile and subsequent association by a 12-fold dilution of the monomeric subunits into aqueous buffer (*9*−*12*). The acetonitrile-induced dissociation rate constant k_d [$4.5 \times 10^{-3}\ s^{-1}$ (*11*, *12*)] monitored by fluorescence is 3 orders of magnitude higher than the dilution-induced dissociation rate constants ($k_{diss} = 2-4 \times 10^{-6}\ s^{-1}$) obtained here, while the fast association rate constant ($k_1 = 2.8 \times 10^4\ M^{-1}\ s^{-1}$) is 4 orders of magnitude higher than our association rate constants ($k_{ass} \cong 1.7\ M^{-1}\ s^{-1}$). A likely explanation of the fast changes (1000 s) in fluorescence is that addition of acetonitrile produces protein unfolding as well as subunit dissociation. Conversely, dilution out of acetonitrile induces fast refolding and slow subunit association. The presence of acetonitrile causes increases in tryptophan and ANS fluorescence intensities (*33*, *34*), which would augment the magnitude of intensity changes; it also causes shifts in the emission spectra. On the other hand, the slow recovery of polymerase activity after dilution into buffer, interpreted as an isomerization rate constant k_2 of $3-6 \times 10^{-5}\ s^{-1}$ (*9*), is only 10-fold higher than the k_{obs} ($3.4-5.8 \times 10^{-6}\ s^{-1}$) values obtained for the equimolar association reactions monitored by enzymatic activity, tryptophan fluorescence, and FRET. At least part of this difference can be attributed to different experimental conditions: pH 8.0 and 25 °C for the published value versus pH 7.0 and 5 °C in this work.

APPENDIX

A488 Fluorescence. The fluorescence of A488 appears to be environmentally sensitive; the intensity of labeled p66 is greater than that of labeled p51 (Figure 4, bottom panel inset). Johnson and co-workers observed a 60−70% decrease in the fluorescence of A488-labeled calmodulin upon binding of a small peptide, which they attributed to the proximity of the fluorescence probe and a Trp residue in the peptide (*35*). We pursued these environmental effects by measuring the fluorescence quantum yield and lifetime of A488-labeled RT monomers and heterodimers as well as *N*-acetylcysteine-A488. Table A1 gives the quantum yield data. The absorption and emission maxima are 488 and 520 nm, respectively, for all A488 conjugates. The p66-A488 monomer has the same quantum yield as labeled *N*-acetylcysteine, which is 3-fold greater than the quantum yield of the p51-A488 monomer. The values of the quantum yield decrease slightly if at all upon dimerization. As expected, the quantum yields of heterodimers containing the donor/acceptor pair are lower than those of heterodimers with donor alone by factors of 8 for p66-A488/p51-QSY9 and 3 for p66-QSY9/p51-A488.

Table A2 gives the fluorescence lifetime data for A488 conjugates. *N*-Acetylcysteine-A488 is a control with no protein interaction. The fluorescence decay is best fit by a biexponential function with a major 4.1 ns component and a minor 0.54 ns component, which has a negative amplitude. A negative term in a fluorescence decay signifies an excited-state reaction with a fluorescent product. The absence of a deuterium isotope effect on the quantum yield suggests that the excited-state reaction does not involve proton transfer (*36*). The fluorescence decays of all RT conjugates gave good fits to three exponential functions with lifetimes of ∼3.6, ∼1, and ∼0.05 ns. The long lifetime of the RT conjugates is shorter than the 4.1 ns lifetime of *N*-acetylcysteine-A488. In all the conjugates, the short lifetime component has the largest amplitude but contributes only ∼2% of the total intensity (Figure A1, top panel). Amplitude-weighted lifetimes ($\bar{\tau}$) of ∼1 ns are calculated from eq 8 (Table A1). The quantum yield drop of A488 in the environment of p66 compared to p51 is accompanied by an ∼1.2-fold increase in amplitude-weighted lifetime. Likewise, the quantum yields of A488-labeled heterodimers decrease in the presence of the QSY9 acceptor, whereas the amplitude-weighted lifetimes increase 1.2−1.3-fold. A quantum yield drop without a parallel lifetime drop is emblematic of static quenching. Static quenching occurs when a species becomes effectively nonfluorescent with intensity or lifetime too small to measure.

The bottom panel of Figure A1 shows the amplitudes of the three lifetime components of the RT conjugates normalized to the steady-state intensity of *N*-acetylcysteine-A488 at 540 nm. We assume that the 3.6, 1, and 0.05 ns lifetimes of the RT conjugates report three ground-state species of A488 in distinct environments and that the same three species occur in all the RT

Table A1: Quantum Yields and Amplitude-Weighted Lifetimes[a]

protein solution[b]	Φ	$\bar{\tau}$ (ns)
0.5 μM p66-A488	0.80 ± 0.02	1.05
2.5 μM p51	0.75 ± 0.05	1.55
2.5 μM p51-QSY9	0.10 ± 0.03	1.37
0.5 μM p51-A488	0.26 ± 0.01	1.23
2.5 μM p66	0.25 ± 0.02	1.41
2.5 μM p66-QSY9	0.079 ± 0.004	1.41
N-acetylcysteine-A488	0.82 ± 0.02	
N-acetylcysteine-A488[c]	0.80 ± 0.02	

[a]RT buffer D, at 5 °C. $\lambda_{ex} = 450$ nm. Errors give the range of average values from two to four experiments. [b]Final concentrations. [c]RT buffer D with D_2O, at 5 °C.

Table A2: Fluorescence Decay Parameters[a]

protein solution[b]	α_1[c]	τ_1[d] (ns)	α_2[c]	τ_2[d] (ns)	τ_3[d] (ns)	χ_r^2
0.5 μM p66-A488	0.24 ± 0.02	3.59	0.17 ± 0.01	0.99	0.035	1.25
2.5 μM p51	0.35 ± 0.02	3.68	0.22 ± 0.02	1.08	0.049	1.31
2.5 μM p51-QSY9	0.31 ± 0.02	3.66	0.20 ± 0.02	1.05	0.046	1.36
0.5 μM p51-A488	0.28 ± 0.01	3.63	0.19 ± 0.02	0.98	0.057	1.21
2.5 μM p66	0.33 ± 0.01	3.51	0.24 ± 0.01	0.93	0.066	1.40
2.5 μM p66-QSY9	0.33 ± 0.04	3.44	0.27 ± 0.01	0.90	0.075	1.29
N-acetylcysteine-A488	0.84 ± 0.01	4.10	−0.16 ± 0.01	0.54		1.30
N-acetylcysteine-A488[e]	0.85 ± 0.03	4.05	−0.15 ± 0.01	0.50		1.35

[a]RT buffer D, at 5 °C. λ_{ex} = 450 nm, and λ_{em} = 540 nm. [b]Final concentrations. [c]$\sum\alpha_i = 1$. Errors in α_i give the range of average values from global analysis of two decay curves. [d]Errors in $\tau_i \sim 5\%$. [e]RT buffer D with D_2O, at 5 °C.

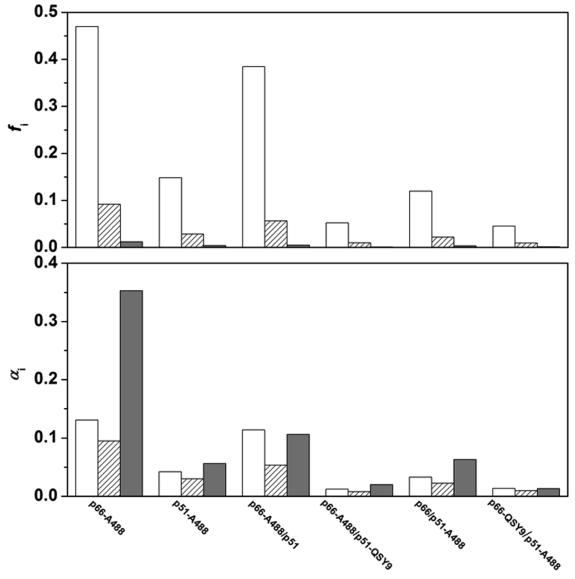

FIGURE A1: Fractional intensities and amplitudes of 3.6, 1, and 0.05 ns decay components of A488-labeled RT monomers and heterodimers: 3.6 ns component (white bars), 1.0 ns component (hatched bars), and 0.05 ns component (black bars). The top panel shows fractional intensities calculated from data in Table A2 using eq 9. The bottom panel shows amplitudes normalized to the steady-state intensity of *N*-acetylcysteine-A488 at 540 nm.

conjugates. Then the quenching of A488 fluorescence in p51 relative to p66 is due to conversion of the three fluorescent species to nonfluorescent species, as seen by the amplitude losses. Tryptophan and to a much lesser extent tyrosine have been shown to quench bimane fluorescence by both dynamic and static quenching mechanisms (*37*, *38*). If bimane and tryptophan are close (10−15 Å), the quenching is dynamic with parallel drops in quantum yield and lifetime. For very close distances (5−10 Å), the quenching is static and only the quantum yield decreases with no change in lifetime. We propose that the 3.6, 1, and 0.05 ns lifetimes of A488 on p66 arise from dynamic quenching by a nearby aromatic residue, possibly W212, which is 5−13 Å from S3 in the crystal structure (*26*). The three lifetimes may arise from different positions of A488 on a 10 Å pentamethylene tether. The static quenching of A488 on p51 would invoke an additional position in which A488 is very close to W212.

The FRET quenching of A488 fluorescence in the two heterodimers with donor/acceptor pairs reflects static quenching due to loss of amplitude, not lifetime quenching. FRET quenching is normally dynamic quenching, which shortens the fluorescence lifetime. For FRET quenching of the A488/QSY9 pair to manifest static quenching, the distance between the donor and acceptor has to be < 30 Å, certainly feasible for two probes on 10 Å tethers.

ACKNOWLEDGMENT

We are grateful to Dr. Michael E. Ignatov for assistance with the pre-steady-state assay and to Ms. Kathryn J. Howard for assistance with the QSY9 labeling reaction. We also thank Dr. Vernon E. Anderson for advice about analysis of the kinetics data and helpful discussions about the reaction mechanisms, Dr. Angela Gronenborn for suggesting model 1, and Dr. Jonathan Karn for critical reading of the manuscript.

REFERENCES

1. Venezia, C. F., Howard, K. J., Ignatov, M. E., Holladay, L. A., and Barkley, M. D. (2006) Effects of efavirenz binding on the subunit equilibria of HIV-1 reverse transcriptase. *Biochemistry 45*, 2779–2789.
2. di Marzo Veronese, F., Copeland, T. D., DeVico, A. L., Rahman, R., Oroszlan, S., Gallo, R. C., and Sarngadharan, M. G. (1986) Characterization of highly immunogenic p66/p51 as the reverse transcriptase of HTLV-III/LAV. *Science 231*, 1289–1291.
3. Kohlstaedt, L. A., Wang, J., Friedman, J. M., Rice, P. A., and Steitz, T. A. (1992) Crystal structure at 3.5 Å resolution of HIV-1 reverse transcriptase complexed with an inhibitor. *Science 256*, 1783–1790.
4. Hizi, A., McGill, C., and Hughes, S. H. (1988) Expression of soluble, enzymatically active, human immunodeficiency virus reverse transcriptase in *Escherichia coli* and analysis of mutants. *Proc. Natl. Acad. Sci. U.S.A. 85*, 1218–1222.
5. Wang, J., Smerdon, S. J., Jager, J., Kohlstaedt, L. A., Rice, P. A., Friedman, J. M., and Steitz, T. A. (1994) Structural basis of asymmetry in the human immunodeficiency virus type 1 reverse transcriptase heterodimer. *Proc. Natl. Acad. Sci. U.S.A. 91*, 7242–7246.
6. Jacobo-Molina, A., Ding, J., Nanni, R. G., Clark, A. D., Jr., Lu, X., Tantillo, C., Williams, R. L., Kamer, G., Ferris, A. L., Clark, P., Hizi, A., Hughes, S. H., and Arnold, E. (1993) Crystal structure of human immunodeficiency virus type 1 reverse transcriptase complexed with double-stranded DNA at 3.0 Å resolution shows bent DNA. *Proc. Natl. Acad. Sci. U.S.A. 90*, 6320–6324.
7. Le Grice, S. F. J., Naas, T., Wohlgensinger, B., and Schatz, O. (1991) Subunit-selective mutagenesis indicates minimal polymerase activity in heterodimer-associated p51 HIV-1 reverse transcriptase. *EMBO J. 10*, 3905–3911.
8. Sluis-Cremer, N., Arion, D., Abram, M. E., and Parniak, M. A. (2004) Proteolytic processing of an HIV-1 pol polyprotein precursor: Insights into the mechanism of reverse transcriptase p66/p51 heterodimer formation. *Int. J. Biochem. Cell Biol. 36*, 1836–1847.
9. Divita, G., Rittinger, K., Geourjon, C., Deleage, G., and Goody, R. S. (1995) Dimerization kinetics of HIV-1 and HIV-2 reverse transcriptase: A two step process. *J. Mol. Biol. 245*, 508–521.
10. Restle, T., Muller, B., and Goody, R. S. (1990) Dimerization of human immunodeficiency virus type 1 reverse transcriptase. A target for chemotherapeutic intervention. *J. Biol. Chem. 265*, 8986–8988.
11. Divita, G., Restle, T., and Goody, R. S. (1993) Characterization of the dimerization process of HIV-1 reverse transcriptase heterodimer using intrinsic protein fluorescence. *FEBS Lett. 324*, 153–158.
12. Divita, G., Rittinger, K., Restle, T., Immendorfer, U., and Goody, R. S. (1995) Conformational stability of dimeric HIV-1 and HIV-2 reverse transcriptases. *Biochemistry 34*, 16337–16346.

13. Wohrl, B. M., Krebs, R., Thrall, S. H., Le Grice, S. F. J., Scheidig, A. J., and Goody, R. S. (1997) Kinetic analysis of four HIV-1 reverse transcriptase enzymes mutated in the primer grip region of p66. Implications for DNA synthesis and dimerization. *J. Biol. Chem. 272*, 17581–17587.
14. Le Grice, S. F. J., Cameron, C. E., and Benkovic, S. J. (1995) Purification and characterization of human immunodeficiency virus type 1 reverse transcriptase. *Methods Enzymol. 262*, 130–144.
15. Ignatov, M. E., Berdis, A. J., Le Grice, S. F. J., and Barkley, M. D. (2005) Attenuation of DNA replication by HIV-1 reverse transcriptase near the central termination sequence. *Biochemistry 44*, 5346–5356.
16. Haugland, R. P. (1995) Coupling of monoclonal antibodies with fluorophores. *Methods Mol. Biol. 45*, 205–221.
17. Molecular Probes. http://probes.invitrogen.com/media/pis/mp00143.pdf.
18. Berdis, A. J., Stetor, S. R., Le Grice, S. F. J., and Barkley, M. D. (2001) Molecular mechanism of sequence-specific termination of lentiviral replication. *Biochemistry 40*, 12140–12149.
19. Wong, I., Patel, S. S., and Johnson, K. A. (1991) An induced-fit kinetic mechanism for DNA replication fidelity: Direct measurement by single-turnover kinetics. *Biochemistry 30*, 526–537.
20. Brannon, J. M., and Magde, D. (1978) Absolute quantum yield determination by thermal blooming. Fluorescein. *J. Phys. Chem. 82*, 705–709.
21. Watrob, H. M., Pan, C.-P., and Barkley, M. D. (2003) Two-step FRET as a structural tool. *J. Am. Chem. Soc. 125*, 7336–7343.
22. Restle, T., Muller, B., and Goody, R. S. (1992) RNase H activity of HIV reverse transcriptases is confined exclusively to the dimeric forms. *FEBS Lett. 300*, 97–100.
23. Baillon, J. G., Nashed, N. T., Kumar, A., Wilson, S. H., and Jerina, D. M. (1991) A leucine zipper-like motif may mediate HIV reverse transcriptase subunit binding. *New Biol. 3*, 1015–1019.
24. Tachedjian, G., Aronson, H. E., de los Santos, M., Seehra, J., McCoy, J. M., and Goff, S. P. (2003) Role of residues in the tryptophan repeat motif for HIV-1 reverse transcriptase dimerization. *J. Mol. Biol. 326*, 381–396.
25. Lakowicz, J. R. (2006) Principles of Fluorescence Spectroscopy, 3rd ed., Springer, New York.
26. Hsiou, Y., Ding, J., Das, K., Clark, A. D., Jr., Hughes, S. H., and Arnold, E. (1996) Structure of unliganded HIV-1 reverse transcriptase at 2.7 Å resolution: Implications of conformational changes for polymerization and inhibition mechanisms. *Structure 4*, 853–860.
27. Kim, S. Y., Byrn, R., Groopman, J., and Baltimore, D. (1989) Temporal aspects of DNA and RNA synthesis during human immunodeficiency virus infection: Evidence for differential gene expression. *J. Virol. 63*, 3708–3713.
28. Schreiber, G., Haran, G., and Zhou, H. X. (2009) Fundamental aspects of protein-protein association kinetics. *Chem. Rev. 109*, 839–860.
29. Zhao, H., and Beckett, D. (2008) Kinetic partitioning between alternative protein-protein interactions controls a transcriptional switch. *J. Mol. Biol. 380*, 223–236.
30. RCSB Protein Data Bank. http://www.rcsb.org/pdb/home/home.do.
31. Seckler, J. M., Howard, K. J., Barkley, M. D., and Wintrode, P. L. (2009) Solution structural dynamics of HIV-1 reverse transcriptase heterodimer. *Biochemistry 48*, 7646–7655.
32. Weikl, T. R., and von Deuster, C. (2009) Selected-fit versus induced-fit protein binding: Kinetic differences and mutational analysis. *Proteins 75*, 104–110.
33. Slavik, J. (1982) Anilinonaphthalene sulfonate as a probe of membrane composition and function. *Biochim. Biophys. Acta 694*, 1–25.
34. Yu, H.-T., Colucci, W. J., McLaughlin, M. L., and Barkley, M. D. (1992) Fluorescence quenching in indoles by excited-state proton transfer. *J. Am. Chem. Soc. 114*, 8449–8454.
35. Slaughter, B. D., Urbauer, R. J., Urbauer, J. L., and Johnson, C. K. (2007) Mechanism of calmodulin recognition of the binding domain of isoform 1b of the plasma membrane Ca^{2+}-ATPase: Kinetic pathway and effects of methionine oxidation. *Biochemistry 46*, 4045–4054.
36. Laws, W. R., and Brand, L. (1979) Analysis of two-state excited-state reactions. The fluorescence decay of 2-naphthol. *J. Phys. Chem. 83*, 795–802.
37. Sato, E., Sakashita, M., Kanaoka, Y., and Kosower, E. M. (1988) Organic fluorescent reagents. XIV. Novel fluorogenic substrates for microdetermination of chymotrypsin and aminopeptidase: Bimane fluorescence appears after hydrolysis. *Bioorg. Chem. 16*, 298–306.
38. Mansoor, S. E., McHaourab, H. S., and Farrens, D. L. (2002) Mapping proximity within proteins using fluorescence spectroscopy. A study of T4 lysozyme showing that tryptophan residues quench bimane fluorescence. *Biochemistry 41*, 2475–2484.